Calibrating fault seal using a hydrocarbon migration model of the Oseberg Syd area, Viking Graben.

C. Childs[1*], Ø. Sylta[2,3], S. Moriya[1,4], N. Morewood[1], T. Manzocchi[1], J.J. Walsh[1], D. Hermanssen[5]

1. Fault Analysis Group, School of Geological Sciences, University College Dublin, Belfield, Dublin 4, Ireland.
2. SINTEF Petroleumsforskning AS, Trondheim, Norway.
3. Migris AS, Trondheim, Norway
4. JAPEX, Tokyo, Japan.
5. Norsk Hydro, Bergen, Norway.

Abstract

It is widely acknowledged that fault rock capillary properties are important in controlling the distribution of hydrocarbons in sedimentary basins, and methods exist for predicting the capillary seal capacity of prospect bounding faults. However, fault seal capacity is rarely incorporated into models of hydrocarbon migration. This paper presents the results of migration modelling of the Oseberg Syd area of the Viking Graben incorporating fault rock capillary properties. Seal capacity is calculated in the model as a function of Shale Gouge Ratio (SGR), i.e. the percentage shale in the sequence moved past a point on a fault. Over 3 000 model realisations were run for different SGR to fault seal capacity relationships and the calculated hydrocarbon distributions were compared with known distributions. Realisations were ranked according to the closeness of fit between model and actual oil-water contacts for 7 traps. The best-fit to all 7 traps was provided by realisations with significant seal capacity at SGR values greater than ca. 0.2; a value which is in agreement with an independently derived fault-by-fault calibration between SGR and seal capacity. The level of fill calculated for an individual trap is extremely sensitive to minor changes in the seal capacity relationship because it is controlled not only by the seal capacities of the faults that bound the trap, but also by the pattern of fill-spill of upstream traps. This sensitivity to minor changes in seal capacity introduces large uncertainties when fault seal capacity relationships are used in a predictive mode and emphasises the requirement for migration modelling in fault seal prospect evaluation.

Keywords: Hydrocarbon migration; fault seal; capillary pressure; migration modelling; SGR calibration

* Corresponding author: Tel: +353 1 7162608 Fax: +353 1 7162607
email - conrad@fag.ucd.ie

1. Introduction

Faults can impede the lateral migration of hydrocarbons by juxtaposing sealing lithologies against reservoir/carrier units or by forming a layer of high capillary threshold pressure fault rock. These two types of seal are commonly referred to as juxtaposition and fault membrane seal respectively. In fault prospect evaluation, juxtaposition seal is evaluated using Allan diagrams showing the across fault juxtaposition of reservoir and sealing lithologies (Allan 1989). Evaluation of fault membrane seal is much more difficult due to the many processes which can result in the formation of high threshold pressure fault rock and the difficulties in predicting their occurrence. In clastic sequences these processes include cataclasis, cementation and shale smearing. Cataclasis and cementation, particularly in combination, can generate very high threshold pressure fault rocks (Gibson 1998; Sperrevik et al. 2002). There are however few reported instances of significant hydrocarbon columns sealed by cataclasis of clean sandstones or cementation (a possible exception is the southern North Sea Rotliegende reservoirs, e.g. Tabor et al. 2003) and to date there are no established methodologies for predicting seal by these processes.

Sealing of reservoir/reservoir contacts in clastic sequences is most commonly attributed to dragging of clay, or shale, into faults to form clay smears (Perkins 1961; Weber 1978; Lindsay et al. 1993; Fulljames 1997; Davis et al. 2003) or shearing of clay rich sandstones (Kim et al. 2003), and in recent years methods for estimating membrane seal potential by these processes have been developed (Bouvier 1989; Fristad et al. 1997; Fulljames 1997; Yielding et al 1997, Bretan et al. 2003). These methods are based on the premise that the seal capacity of a fault separating juxtaposed reservoirs is a function of the shale content of the offset sequence. A number of different expressions of shale content have been calibrated empirically against oilfield data to provide a means for predicting seal capacity in fault bound prospects (Yielding et al 1997). While there is no consensus on the preferred form of these expressions there is widespread agreement that the basic assumptions and methodologies are widely applicable to seal evaluation (but see James et al. 2004 for opposed view). Despite the acknowledged importance of fault

membrane seal and the availability of methods for its estimation, membrane seal is not routinely incorporated into hydrocarbon migration models. In this paper we outline refinements to a methodology for incorporating the capillary sealing properties of faults into migration modelling originally described in Childs et al. (2002). Applying the method to the Oseberg Syd area of the Viking Graben we demonstrate how this approach provides an objective means for defining fault seal predictors and the uncertainty attached to these predictors in terms of trapped oil column heights.

2. Oseberg Syd

The Oseberg Syd area lies within Norwegian Block 30/9 on the eastern flank of the North Viking Graben (Fig. 1). The area comprises a series of fault blocks rotated to the east and bounded by large (throws up to 300m) west-dipping, normal faults of Late Jurassic age. The area contains several known hydrocarbon accumulations proven in ~ 22 wells. Hydrocarbons occur within the Jurassic Tarbert and Ness Formations and the Triassic Statfjord Formation. Within the Jurassic, the majority of proven hydrocarbons occur within the Tarbert reservoir with relatively minor volumes in the deeper Brent section in the BN and ON blocks (Fig. 1(B)). In the northern part of the study area the Tarbert Formation is locally eroded on the footwalls of large faults. In this paper we are concerned only with hydrocarbon distribution within the Tarbert Formation. Across-fault thickness changes of the Tarbert Formation demonstrate that some faults within the study area were active during Tarbert deposition.

Hydrocarbon accumulations within the Oseberg Syd field all depend to some extent on fault membrane seal and several low-side traps rely entirely on fault-membrane seal. A migration model of the area, which does not include fault rock capillary properties is shown in Fig. 2. This model is identical to those described later in every respect except that the capillary sealing effects of fault rock are not included. Comparing this map with the known hydrocarbon distributions (Fig. 1(B)), it is clear that fault membrane seal is required to explain the observed hydrocarbon distribution. Oseberg Syd is therefore an ideal area for examining both fault seal effects in migration modelling and for testing fault seal predictors in migration models.

Fault seal within the Oseberg Syd area was previously studied by Fristad et al. (1997). These authors mapped both across-fault pressure differences and Shale Gouge Ratio (SGR - the proportion of shale in the sequence which has moved past a point on a fault) over fault surfaces. For each fault they constructed cross-plots of pressure difference against SGR to determine the point on the fault which was likely to control seal capacity, i.e. the point with the highest ratio of pressure difference to SGR. Performing this exercise for several faults they established an empirical dataset of SGR against pressure difference to define a seal capacity envelope for the faults in Oseberg Syd which could be used as a predictor of seal capacity in fault bound prospects; they found that significant fault seal occurred at SGR values greater than 0.18 (or 18%). A similar calibration exercise was conducted in this study (Fig. 3), but here we have calibrated SGR against capillary pressure due to the buoyancy of the trapped hydrocarbon columns, rather than across fault pressure difference, since the latter is due to both buoyancy and hydrodynamic effects. The capillary pressure *(P_c)* is calculated as

$$P_c = (\rho_w - \rho_o)gh$$

where ρ_o and ρ_w are oil and water density respectively and h is height above the oil-water contact. Where hydrocarbon columns occur on both sides of a fault, h is height above the deeper of the two oil-water contacts (Childs et al, 2002). Despite this difference the results of the study performed here and those of Fristad et al. are very similar and onset of significant seal occurs at SGR values of 0.15 to 0.2. In addition, the calibration for the oil columns suggests a positive correlation between SGR and seal potential. Revisiting the study of Fristad et al., Bretan et al. (2003) demonstrated that the SGR value at the point of onset of significant fault seal varies with the method used for calculating Vshale. It is therefore crucial that consistent methods for calculating Vshale are used throughout an empirical seal capacity dataset. The Vshale logs used here are the same as those used by Fristad et al. so that comparing results between the two studies is valid.

The calibration dataset derived here, like that of Fristad et al. (1997), suggests that higher buoyancy pressures can be supported for gas columns than oil columns. This is to be expected given that in a water-wet system gas threshold pressures are higher than those for oil, due to the higher interfacial tension in the gas-water system. However higher gas threshold pressures are not necessarily reflected in higher gas columns due to

the lower density of gas (Heum, 1996). In the modelling described here we concern ourselves only with oil distribution for reasons described below. The fault seal envelope for oil derived from the data is later compared with that derived from migration modelling.

3. Methodology

3.1. Description of migration simulator

There are several simulators available that can simulate the basin scale flow of oil and gas during geological times, both commercial and academic (see e.g. Carruthers & Ringrose, 1998, Johannesen et al., 2002, Kauerauf et al, 2007). All basin scale flow simulators have so far been rather simplistic in their treatment of faults, both in terms of geometric descriptions and flow modelling. The simulator chosen uses a ray tracing technique in which hydrocarbons migrate upwards under the influence of buoyancy, as stringers or rivulets along the top of the reservoir (or carrier) interval. Flow within simple non-vertical fault planes can be simulated, and faults can be assigned fault seal properties. Hydrocarbons are trapped within structural closures of the top reservoir surface, spilling from the base of a trap, when the base of the hydrocarbon column reaches the structural spill-point, to fill structurally higher traps (Sylta, 1991; Krokstad and Sylta, 1996). The top reservoir horizon and the reservoir thickness distribution are represented as grids within the simulator. Definition of Vshale within the model, which is used in the calculation of SGR values, is described below. Faults are input as polygon maps and fault throws are calculated within the simulator from horizon elevation changes across fault polygons. Hydrocarbon charge can be either calculated within the simulator, from source bed thickness grids and equations defining standard kinetic reactions, or hydrocarbon volumes calculated outside of the simulator can be injected during a model run. The simulator tracks spatial and temporal variations in hydrocarbon composition and phase throughout a model run. Although the simulator can perform modelling within several reservoir intervals, in this study we model only one reservoir interval.

3.2 Incorporation of fault seal within the migration simulator

Three types of fault seal behaviour are incorporated in the migration simulator (Fig. 4; Childs et al. 2002), juxtaposition seal, cross-fault membrane seal and along-fault membrane seal. Juxtaposition seal is defined by the geometry of the top of the faulted reservoir, and hydrocarbons will fill the upthrown side of a fault until the oil-water contact reaches the highest point of across-fault, reservoir-reservoir juxtaposition (Fig. 4(A)). Cross-fault membrane seal, due to the sealing capacity of the layer of fault rock between juxtaposed reservoir sections, is calculated as a function of the SGR distribution on the fault surface as illustrated in Fig. 4(B). At any point along the length of a fault the SGR curve for the area of across-fault reservoir juxtaposition is calculated from the fault throw and the Vshale distribution within the sequence at that location. The SGR curve is then converted to a fault rock capillary threshold pressure curve (Childs et al. 2002) using a defined relationship (see below). The membrane seal capacity at a point along a fault trace is defined by the oil-water contact level at which the capillary pressure curve touches the capillary threshold pressure curve for the fault (Fig. 4(B)). The relationship between SGR and capillary threshold pressure can be derived from oilfield calibration datasets such as that in Fig. 3. A relationship can also be derived from laboratory measurements of fault rock threshold pressure and phyllosilicate fraction, if it is assumed that fault rock phyllosilicate fraction is related to SGR on the fault surface. Laboratory data are usually derived from mercury/air injection experiments. Transferring these results to consideration of fault seal requires a knowledge of the hydrocarbon-water interfacial tension at subsurface conditions which are often poorly constrained. In this paper we input a range of different SGR to threshold pressure relations as described below.

The along-fault membrane seal capacity, where the fault throw is larger than the thickness of the reservoir section, is found from the fault rock threshold pressure curve derived from the SGR distribution at a point along the length of a fault (Fig. 4(C)). In this case hydrocarbons are assumed to migrate up, or down, the fault once the capillary pressure due to the trapped column of oil exceeds the maximum fault rock threshold pressure along the fault trace separating the reservoir section on the upthrown and downthrown sides of the fault. This method contrasts with that used by Childs et al

(2002) where oil was allowed to migrate both vertically and laterally over the fault surface following tortuous paths of lowest threshold pressure. Although the approach of Childs et al. is more realistic, the results of the present study are not significantly affected by adopting the simpler approach shown in Fig. 4c. Where fault throws are greater than the thickness of the Tarbert Formation, the upthrown and downthrown reservoir sections are separated by a swathe of high SGR values. These SGR values are relatively uniform on fault dip sections but are much more variable along strike due to changes in throw and Vshale. Tortuous, low threshold pressure pathways over fault surfaces are therefore not significant for this study and the minimum of the seal capacities calculated at points along the length of a fault using the approach shown in Fig. 4c is a reasonable approximation of the approach used by Childs et al. 2002.

The seal capacity at all points along the length of a fault is defined from the juxtaposition, cross- or along-fault membrane seal capacity for a range of hydrocarbon densities and trapped phases (gas and/or oil). For a particular hydrocarbon trap and hydrocarbon density, the simulator identifies the weakest point on the bounding fault surface(s) and hydrocarbons escape from the trap at that point once the hydrocarbon column attains the seal capacity. Hydrocarbon will continue to leak from this point until the trap is no longer charged or until a change in hydrocarbon density or phase causes a different leak point to be activated. The model does not include the effects of capillary hysteresis and we assume ‘snap-off’ of the oil phase within the fault occurs at the fault rock threshold pressure so that the capillary seal capacity of the leak point after leakage is the same as before leakage occurred. Some workers estimate that the seal capacity of a fault may be reduced by a factor of 2 to 4 following capillary leakage (Brown 2003) in which case a consideration of capillary hysteresis clearly would have a profound effect on how we conceptualise SGR – fault seal relationships. However whether trapped columns are stable at the threshold pressure of the fault rock or at some point on the fault rock capillary pressure imbibition curve is of little importance for defining a fault seal calibration.

4. Oseberg model construction and model parameters

The Oseberg model construction and application were designed specifically to examine the effect of varying the fault seal capacity predictor on hydrocarbon distribution and to determine which relationship between SGR and fault rock threshold pressure best replicates known hydrocarbon distributions. In this study we are not therefore concerned with the full range of parameters and parameter uncertainties which would normally be defined in a migration risking study e.g. source rock kinetics, thermal history etc (e.g. Sylta 2004). Some of the model inputs are therefore simplified to remove degrees of freedom in parameters unrelated to fault seal capacity. On the other hand, attention has been paid to define, as accurately as possible, those parameters which impact fault seal capacity, i.e. fault throw and Vshale distribution.

4.1. Geological model

The geological model is defined from 5 horizons (Fig. 5) and 22 wells (Fig. 1). The fault map pattern (Fig. 2) is from the seismically mapped mid-Tarbert reflection. The fault map pattern is the same on each of the 5 horizons, so that faults are represented in the model as vertical zones equal in width to the heave polygon mapped on the mid-Tarbert (Fig. 5). The key horizon for migration modelling purposes is the top of the Tarbert reservoir, which differs from the Top Tarbert Formation in that the upper parts of the Tarbert Formation are not of reservoir quality in the western part of the area. The Tarbert Formation is locally eroded at the Base Cretaceous Unconformity so that offsets of the top Tarbert reservoir do not reflect the pre-erosion fault throws which are required to calculate SGR values. Appropriate fault throws were derived from a base Tarbert horizon modified to account for local erosion by extrapolation across the unconformity.

The model is populated with Vshale values calculated using a distance-weighted interpolation from wells and guided by mapped horizons. Faults which were active during deposition and across which there are step changes in thickness and facies/Vshale content are included as breaks in the interpolation. Where there is a single well within a block bounded by syn-depositional faults, the Vshale curve for that well is assigned to the whole block with adjustments for spatial variations in interval thicknesses.

4.2. Migration history

Faulting in the Viking Graben occurred in the Mid to Late Jurassic. Active extension was followed by passive thermal subsidence (Badley et al. 1984). The basin has continued to subside, with some significant hiatuses, to the present day. There has been a long history of hydrocarbon generation in the area which may have started in the Late Cretaceous in the deeper parts of the basin (Dahl 1987) and is likely to continue to the present. The source beds for hydrocarbons are the Draupne and the Heather Formations which overlie the Tarbert reservoir section. The source rocks within the study area have not been buried to the depths required for hydrocarbon generation. Regional scale migration modelling indicates that hydrocarbons that occur within reservoirs in the study area are sourced from kitchen areas in all directions, with the main kitchen areas to the south, west and north. In this study we attempt to model only those hydrocarbon accumulations which lie to the west of the Oseberg Fault (OF in Fig. 1). We do not attempt to model the J structure (marked JC1 and JN and JW2 on Fig. 1), partly because it is an area of intense erosion and the structure and fault offsets are poorly defined, but primarily because this structure forms the highest closure in the area, so that the level of fill in this structure is hydrocarbon charge or top seal dependent rather than fault controlled. The Oseberg Field straddles the northern edge of the model area so that migration into this trap cannot be studied in the model. Geochemical evidence suggests that the hydrocarbons of the C structure (Fig. 1) are the same as those of the main Oseberg structure and part of a migration system sourced from the north. These accumulations are unrelated to those west of the Oseberg Fault which are sourced from the west and the south.

The hydrocarbons in the study area are predominantly oil with an increasing proportion of gas towards the west. We have only incorporated oil in our modelling to reduce the number of controls on the hydrocarbon accumulation history. Inclusion of the gas phase would require investigation of the uncertainties associated with the relative timing and volumes of oil and gas generation and would detract from the central aim of examining fault seal capacities; the significance of excluding the gas phase is discussed below. A constant volume of oil, sufficient to fill all available traps, is injected into the

model. The oil is injected into the reservoir at the margins of the model, at locations and relative proportions defined from a larger scale regional model. Oil that is not trapped within accumulations to the west of the Oseberg Fault migrates to the highest structure in the area, i.e. the J structure, and eastwards out of the model once the geometric closure of the J structure is exceeded. The level of fill within the J structure is therefore determined by the volume of oil injected into the model and contains no information on fault seal capacities.

4.3. Fault seal case definition

A total of 3 130 different model realisations were defined by varying the relationship between SGR and fault rock threshold pressure i.e. the fault seal capacity envelope or fault seal predictor. The seal capacity envelopes are of the form shown in Fig.6. Onset of fault sealing (non-zero threshold pressure) occurs at a particular SGR cut-off (referred to here as SGR-onset), the threshold pressure increases linearly with a defined slope, until it reaches a maximum threshold pressure value. Values for the SGR-onset, slope and maximum threshold pressure for each fault seal realisation are randomly sampled between defined limits, which for the Oseberg Syd study are 0 to 0.4, 0 to 250bars (per unit SGR), and 0 to 25bars, respectively. A second set of 835 realisations was generated in which the inclined section of the seal capacity envelope was replaced with a concave upwards curve.

4.4. Model calibration

The degree of fit between model and actual oil distributions is determined by the heights of the trapped oil columns. Column height is measured as the vertical interval from a calibration point located at a trap crest to the oil-water contact. Calibration points are located at the crest of seven traps in the area of interest, i.e. west of the Oseberg Fault (open circles in Fig. 2). For clarity of description throughout this paper the column height at a calibration point is synonymous with the column height in an associated trap; however, it is important to note that the associated trap cannot be outlined on a map since the area of the equivalent ‘trap’ varies between model realisations and adjacent traps may

merge when the oil-water contact is deeper than the spillpoint separating them. For individual traps (or calibration points), a negative misfit indicates the model oil-water contact is shallower than the actual contact and a positive misfit indicates that the model accumulation is overfilled. The total misfit for a particular realization is the sum of the absolute values of misfit for all seven traps. Weightings according to trapped oil volumes are not applied in calculation of the total misfit as the important measure is buoyancy due to column height which is independent of areal extent. Calculation of misfit on the basis of column height was chosen as it makes best use of the available data. Alternative approaches based on, for example, oil encountered in wells, would not provide as good a measure of fit, as wells will rarely intersect the oil water contact so that calibration would be mainly against oil-down-to and water-up-to data. While the approach adopted here avoids bias towards larger traps on the basis of volume or number of wells per trap, there is a bias in the misfit calculation towards higher oil columns as these can record a more significant misfit when underfilled.

Although we model only oil migration, three of the calibration points are located within pools containing both oil and gas (Fig. 1). In each of these pools the gas cap is relatively small. In two of the pools (the GE and K structures, Fig. 1) the gas-oil contact is shallower than the geometric seal capacity of the trap and the presence of the gas cap has no effect on fault seal. In the third of these traps, GC, it is possible that gas occurs at a potential across-fault leak point and this may introduce incorrect column height calculations into the model. As discussed above, the higher threshold pressures associated with a gas-water system relative to an oil-water system are largely balanced by the higher buoyancy of a gas column relative to an oil column of the same height, so that the net effect on column heights is minimal. However where an oil column has a thin gas cap at a potential across fault leak point, the buoyancy force due mainly to the oil column will act on a gas capillary threshold pressure so that the oil column would (at least theoretically) be significantly larger (~ a factor of 2) than would be the case in the absence of the gas cap (Watts, 1987). It is therefore possible that column heights for the GC accumulation in the modelling are lower than would be the case if the gas phase was also modelled.

5. Results

5.1. Individual traps

The misfit associated with each of the seven calibration points for the 3 130 realisations are shown on a plot of SGR-onset against slope (Fig. 7). The pattern of misfit distribution associated with the different traps is varied and depends on the structural setting of each culmination. The misfit pattern associated with Trap 2 is the simplest as it depends almost entirely on the seal capacity of its associated sealing fault. When this fault has a high seal capacity, i.e. realisations with low SGR-onset and high slope, the trap is overfilled (positive misfit), when it has a low seal capacity the trap is underfilled (negative misfit) and there is an intervening parameter range over which the misfit is close to zero. Traps which are further to the east and structurally higher than Trap 2 receive their hydrocarbon charge by leakage from other traps and therefore have complicated misfit distributions. The general pattern of these distributions is a band of low, positive or negative, misfit surrounded by high negative misfit values (traps 1, 3, 4 and 5). This misfit pattern arises because, for parameter ranges providing high seal capacities, the trap may not be charged as oil is deflected by sealing faults further down flank. This is illustrated for Trap 5 (block ON) where oil charge from the kitchen area to the west is deflected to the south because of high seal capacity associated with a fault downflank (Fig. 8(A)). When seal capacities are low then bounding faults do not trap the incoming hydrocarbons, as illustrated by the leakage across the eastern bounding fault to Trap 5 in Fig. 8(C). The low misfit parameter ranges for these traps correspond to seal envelopes which balance the requirement for faults to have seal capacities low enough to allow oil to access the trap but high enough to retain that oil (Fig. 8B). Traps 2 and 5 illustrate the general forms of misfit distribution that occur, but the patterns associated with individual traps have additional complexities superimposed on these basic patterns due to activation of different across-fault leak points and switching of migration arteries. A feature of the plots in Fig. 7 is that the curves separating different misfit bins slope gently to the left at low SGR values, becoming vertical at SGR values in the range 0.15 to 0.3. This curve shape reflects the fact that equivalent fault seal capacities can be achieved

with low values of SGR-onset and low slopes or high values of SGR-onset and high slopes. i.e. the curve defines a range of seal capacity envelopes that intersect at a point.

The graphs in Fig. 7 ignore the third parameter defining the seal capacity envelope i.e. the maximum threshold pressure. The bands of data within the different misfit bins in Fig. 7 are 2D projections of curved surfaces in the 3D parameter space. The significance of the third parameter is seen by the degree of overlap between misfit bins on the plots of SGR-onset against slope. The generally sharp boundaries between different misfit categories demonstrate that the combination of these parameters provides a better discriminator between misfit bins than either one combined with maximum threshold pressure. Low misfit outliers which lie above and to the left of the main band of low misfit data, in for example 1, 2, 3 and 7, occur because the maximum threshold pressure in these realisations is at the particular value required to yield the optimal seal capacity at critical points on the controlling faults. The level of fill in these cases is independent of both the slope and the SGR-onset in the upper left parts of these figures and these seal capacity envelopes yield the same result as would be achieved with constant threshold pressure realisations.

5.2. All traps

Figure 7 shows that there are similarities in the misfit distributions of the different traps and the minimum misfits occupy similar regions of the SGR-onset/slope parameter space. However, the locations of the misfit minima vary and a single parameter range which yields the best fit for all traps does not exist. To define the range of best-fit seal capacity envelopes for the system as a whole we use a measure of the total misfit, calculated as the sum of the absolute values of the misfits of the individual traps (Fig. 7). The relationships between the total misfit and the three parameters defining the seal capacity envelope are shown in Fig. 9. Low misfits are obtained for SGR-onset values in the range 0.15 to 0.25, with the lowest values of 250 m obtained at SGR-onset of 0.18. The minimum attainable misfit decreases with increase in both the slope and the maximum threshold pressure up to values of 80 bars and 6 bars respectively above which the minimum misfit remains approximately constant.

All realisations of the seal capacity envelope are shown on Fig. 10 (A) and colour coded according to misfit. The lowest misfit relationships (<400 m) occur within a narrow zone centred on SGR values of c. 0.2. These best-fit relationships occur within a similar area of the plot as the data derived from the standard single-fault seal calibration approach (Fig. 3), indicating a degree of consistency of results between the two approaches. However, there are differences in the two results and a best fit line drawn through the single-fault calibration datapoints is significantly shallower than the minimum misfit relationship derived from the modelling.

5.3. Sensitivity analysis and trap evaluation

The misfit data (Fig. 7) show that there are differences in the best-fit seal capacity envelopes for different traps. The data also demonstrate that the level of fill in individual traps can be extremely sensitive to minor variations in the seal capacity envelope, for example, envelopes which give a good match for Trap 5, with misfit less than 10m, occur immediately adjacent to relationships which result in underfilling of the trap by more than 100m. In these circumstances the application of a single input seal capacity relationship will result in very large misfits for one or more traps. Use of a fault seal capacity envelope to predict the fill of fault bounded prospects therefore requires a rigorous analysis of sensitivities. Here we examine the sensitivity of the predicted oil columns to variations in the seal capacity envelope for each of the seven traps. Each trap in turn is considered to be a prospect with an unknown column height. For all 3130 realisations, the total column-height misfit is calculated for the six remaining traps. The 200 model realisations with the lowest total misfit are then used to produce histograms of predicted column height in the prospect. These histograms are shown for all seven prospects in Fig. 11.

The form of the histograms associated with each trap reflects the pattern of fault controlled migration arteries which are activated, or deactivated, within the range of seal capacity envelopes defined by the 200 best-fit relationships. Separate peaks in an individual histogram relate to leakage from the trap at different locations either along the length or down the dip of the trap bounding fault. For example, there are two fault

controlled spill-points defining the level of fill in Trap 7. One of these spill-points is stable over a range of seal capacities as demonstrated by variations in the calculated column height from 180 to 260m, while the other is activated over a more limited range of seal capacities i.e. it is capable of sealing an oil column of c. 80m. For three of the traps (1, 3 and 5) a significant proportion of the 200 realisations yield zero column height due to a lack of charge. The different forms of the histograms clearly have different implications from the point of view of risking trapped column heights. The unimodal, although extremely broad, distribution of Trap 2 predicts that hydrocarbons will be encountered but there will be large uncertainty in the level of fill, while Trap 4 is likely to follow one of two scenarios resulting in very different but well defined column heights.

The actual column heights for individual traps (arrowed in Fig. 11) do not always lie within the range defined for the 200 best fit realisations because the best fit parameter range for an individual trap does not necessarily overlap with the range for the remaining six traps. This can be appreciated by comparing, for example, the misfit distribution for Trap 3 with the best fit parameter range for the remaining traps outlined in Fig. 7. The outlined area encloses only realisations where Trap 3 is either not filled or overfilled, although there are realisations at the margins of the outlined range where Trap 3 is within 10m of the actual column height. If the histograms in Fig. 11 were defined from the 300 best fit realisations, then the actual column height for Trap 3 would be included within the range.

6. Discussion

6.1 Fault seal prediction

The data presented in Figs 7 and 11 provide a means for calibrating a fault seal capacity envelope and for examining the sensitivity of calculated oil column heights to variations in seal capacity. A method for defining the most likely fill scenario has not been presented because the optimal method will vary depending on a variety of factors, including the number of wells, the uncertainty in structural mapping etc. However, to allow us to compare predictions based on our model results against actual column heights, we use a very simple approach to defining a predicted column height from the

histograms in Fig. 11. We consider the modal values derived from the peak that contains the most data in the histogram for each trap as indicating the most likely fill scenario. These data are plotted against the actual column heights for each trap in Fig. 12 (A). The plot shows a positive correlation between the predicted and the actual with relatively close agreement for several of the traps. While this correlation suggests that the methods and approaches described here can form a basis for constraining estimates of fault bounded trap capacity, the ranges in predicted oil columns for each trap emphasise the uncertainty in predicted columns, even for the 200 best-fit seal capacity envelopes.

Our ‘misfit’ approach to ranking realizations, as discussed above, is one of a range of methods which could be applied in prospect evaluation. Another approach would be to utilise the strong interdependencies that can arise between pairs or groups of traps that could provide a basis for scenario based evaluation of prospects. An example of this type of approach is illustrated in Fig. 12(B) using the interdependence between the column heights in Traps 2 and 4 for each of the 3 130 straight-line seal capacity relations shown in Fig. 10(A). Although this plot demonstrates a complex relationship between these two traps, reflecting the switching on and off of migration pathways between them, there are some simple observations which can be made. Trap 4 is the structurally higher of the two traps and frequently receives its charge from Trap 2, as shown for instance in Fig. 8B (although this is not the case for example where the column height in Trap 2 is zero and that in Trap 4 is up to 100 m). If the level of fill in Trap 4 is known it can place strong constraints on the column height in Trap 2, for example if the column height in Trap 4 is 150 m then Fig. 12 (B) would predict that Trap 2 would have a column height of ca. 100 m. The level of fill in Trap 2 however does not depend on charge from the structurally higher Trap 4, and a zero column height in 4 can correspond with the full range of possible column heights in 2. Therefore a prediction of the column height in Trap 4 based on a known Trap 2 column height would be ambiguous. The open circle in Fig. 12(B) shows the actual column heights for the two traps and the implications for prediction of one of the column heights if the other were known can be seen.

In this study we have considered only the sensitivity of hydrocarbon distribution to fault seal capacity. This is only one of the many factors which would be considered in a complete sensitivity for prospect evaluation which would include uncertainty in

geological mapping, source rock chemistry, burial history etc. The inclusion of these other sources of uncertainty would have the effect of smoothing through many of the abrupt changes column height with change in seal capacity shown in Fig. 7.

6.2. Fault seal calibration

A migration modelling approach to fault seal capacity calibration and the more conventional approach, based on mapping SGR and buoyancy pressure over fault surfaces, have both been applied to the Oseberg Syd data. The results of the two approaches yield similar results (Fig. 10A), suggesting there is onset of fault seal at SGR values in the range 0.15 to 0.2, with rapid increase in seal capacity at higher SGR values; this result is in agreement with a previous study of fault seal in the Oseberg Syd area (Fristad et al. 1997). In detail however the results are different, with a steeper best-fit relationship derived from the migration modelling. The steep relationship defined by the migration modelling supports the application of an SGR cutoff, above which there is significant seal, rather than a positive correlation between SGR and seal capacity suggested by the standard approach (Fig. 3). Because hydrocarbon distributions are so sensitive to relatively minor changes in seal capacity envelope, the differences between the two results, may be significant in prospect evaluation. There are several possible reasons why the two approaches yield different results because the two methods are based on slightly different versions of the horizon mapping, SGR mapping onto faults and methods for interpolating Vshale through the model volume. A possible reason why the standard approach might yield lower slopes than the migration modelling approach is the subjectivity in defining the leak point of a trap inherent in the standard approach. Faults which offset a shaling upwards sequence will define a positive correlation between SGR and capillary pressure i.e. both will increase upwards on a trap bounding fault. In these situations it is difficult to make an objective decision as to which is the leak point across the fault, and there may be a tendency to consider the high capillary pressures at the top of the trap to be the leak point. In these circumstance the SGR at the interpreted leak point will be higher than if leakage is considered to have occurred at the base of the oil accumulation. If this procedure is repeated for several accumulations it will result in an inclined rather than steep seal envelope.

The data presented in Fig. 7 demonstrate the complex relationship between trapped column height and fault seal envelope and the differences in this relationship for different traps. The pattern of this variability for an individual trap is defined not only by the seal capacity of the trap bounding fault(s) but also the sealing behaviour of upstream faults. The calibration of seal capacity using a migration modelling approach acknowledges and implicitly incorporates all of this complexity and should therefore result in a more robust result than the standard approach to seal calibration.

6.3. Fault seal capacity envelope

In this study we have assumed a straight line relationship between SGR and fault rock threshold pressure. To investigate the extent to which this assumption predetermines our results, a second set of 835 realisations was run using a different shape SGR to threshold pressure relationship (Fig. 10B). These relationships were defined by an SGR-onset and a maximum threshold pressure as before, but the inclined section of the seal capacity envelope (see Fig. 6) was replaced by a concave upward curve. This shape was chosen as it allows for the possibility of some seal capacity, due to porosity collapse and/or cataclasis in clean sands, at SGR values below those generally associated with the onset of seal by clay smearing. The results of this second set of analyses are shown in Fig. 10(B). The fit to the known hydrocarbon distributions achieved in these realisations is not as good as with the straight line relationship, with only two of the 835 realisations having misfits lower than 400m. The 2 best fit realisations for the curved relationship have SGR onset values of ~0.2, are very steep and, on the plot of SGR against threshold pressure, lie within the range of low misfit (< 400m) defined for the straight line relationship (Fig. 10A). We conclude that the more complicated curved seal envelope does not improve the match to the data and the use of straight line seal capacity envelopes is justified.

Both the worsening of the fit to the known column heights with the curved seal capacity envelope and the SGR onset values of 0.2 for both the straight and curved seal capacity relationships suggests that porosity collapse/cataclasis in clean sands (< ca 15% clay) does not contribute significantly to fault seal capacity in this area. An SGR-onset value of 0.2 is consistent with core observations that clay-poor faults in the Tarbert

Formation are disaggregation zones rather than cataclasites. The same onset value was obtained by single-fault calibration in the Columbus Basin (Gibson and Bentham 2003). Although our results suggest that a straight line relationship between SGR and seal capacity provides the best match to available data, we cannot rule out the possibility that other fault seal algorithms, for example those based on continuous shale smearing, would not produce a better fit to the data; an investigation of the full range of potential algorithms was beyond the scope of this study. The very steep seal envelope obtained from our modelling does lend support to the application of a cutoff between non-seal and significant sealing, which is the basis for algorithms that consider fault sealing to be controlled by clay smear continuity.

7. Conclusions

Incorporating fault rock capillary threshold pressures into migration modelling provides an objective means of finding the optimal fault seal envelope for matching known hydrocarbon distributions. Calibration of fault seal envelopes using the migration modelling approach requires, not only matching the sealing capacities of individual faults, but also the network of migration arteries which provides hydrocarbon to fault bounded closures. For the Oseberg Syd area, a good match between model and actual oil distributions is achieved allowing confident definition of the range of best-fit seal capacity envelopes. This range of envelopes is in broad agreement with the results of standard calibration techniques with onset of fault seal at SGR values in the range 0.15 to 0.2. The migration modelling results highlight the complex sensitivities of trap fill to fault seal properties which arise in a system where oil migration is focused by faults. In the Oseberg Syd area these sensitivities are reflected in polymodal frequency distributions of modelled column height.

Acknowledgements

This work was funded by the EC Joule III Programme (Contract No. ENK6-CT-2000-00072). We thank staff at Norsk Hydro, Bergen for provision of data. Peter Boult and an

anonymous reviewer are thanked for their helpful comments.

References

Allan, U. S. 1989. Model for hydrocarbon migration and entrapment within faulted structures. AAPG Bulletin, 73(7), 803-811.

Badley, M. E., Egeberg, T., Nipen, O. 1984. Development of rift basins illustrated by the structural evolution of the Oseberg feature, Block 30/6, offshore Norway. Journal of the Geological Society, London. 141, 639-649.

Bouvier, J. D., Kaars-Sijpesteijn, C. H., Kluesner, D. F., Onyejekwe, C. C., Van Der Pal, R. C. 1989. Three-dimensional seismic interpretation and fault sealing investigations, Nun River Field, Nigeria. AAPG Bulletin, 73(11), 1397-1414.

Bretan, P., Yielding G., Jones, H., 2003. Using calibrated shale gouge ratio to estimate hydrocarbon column heights. AAPG Bulletin, 87 (3), 397-413.

Brown A. 2003. Capillary effects on fault-fill sealing. AAPG Bulletin, 87 (3), 381–395.

Carruthers, D., Ringrose, P., 1998. Secondary oil migration: oil-rock contact volumes, flow Dating and Duration of Fluid Flow and behaviour and rates, in: Parnell J. (Ed), Fluid-Rock interaction, Geological Society London Special Publication, 144 pp. 205-220.

Childs, C., Sylta, Ø., Moriya, S., Walsh, J.J., Manzocchi, T. 2002. A method for including the capillary properties of faults in hydrocarbon migration models, in: Koestler, A.G., Hunsdale, R. (Eds), Hydrocarbon Seal Quantification. Norwegian Petroleum Society (NPF), Special Publication 11, pp. 187-201.

Dahl, B., Nysaether, E., Speers, G. E., Yukler, A. 1987. Oseberg area-integrated basin modeling, in: Brooks, J., Glennie, K. W. (Eds), Petroleum geology of north west Europe: London, Graham & Trotman. pp. 1029–1038.

Davies, R. K, An, L., Jones, P., Mathis, A., Cornette, C. 2003. Fault-seal analysis South Marsh Island 36 field, Gulf of Mexico. AAPG Bulletin, 87(3), 479-491.

Fristad, T., Groth, A., Yielding, G., Freeman, B. 1997. Quantitative fault seal prediction - a case study from Oseberg Syd, in: Møller-Pedersen, P. & Koestler, A. G. (Eds), Hydrocarbon Seals - Importance for Exploration & Production. Norwegian Petroleum Society (NPF), Special Publication 7., Trondheim, Norway, pp. 107-124.

Fulljames, J. R., Zijerveld, L. J. J., Franssen, R. C. M. W. 1997. Fault seal processes: systematic analysis of fault seals over geological and production time scales. in: Møller-Pedersen, P. & Koestler, A. G. (Eds), Hydrocarbon Seals - Importance for Exploration & Production. Norwegian Petroleum Society (NPF), Special Publication 7., Trondheim, Norway, pp. 51-59.

Gibson, R. G. 1998. Physical character and fluid-flow properties of sandstone-derived fault zones, in: Coward, M. P., Daltaban, T. S. & Johnson, H. (Eds), Structural Geology in Reservoir Characterisation. Geological Society, London. Special Publication, 127, pp. 83-97.

Gibson, R. G., Bentham, P. A. 2003. Use of fault-seal analysis in understanding petroleum migration in a complexly faulted anticlinal trap, Columbus Basin, offshore Trinidad. AAPG Bulletin, 87(3), 465-478.

Heum, O. R. 1996. A fluid dynamic classification of hydrocarbon entrapment. Petroleum Geoscience, 2, 145-158.

James, W. R., Fairchild L. H., Nakayama, G. P., Hippler, S. J., Vrolijk, P. J. 2004. Fault-seal analysis using a stochastic multifault approach. AAPG Bulletin, 88(7), 885-904.

Jev, B. I., Kaars-Sijpesteijn, C. H., Peters, M. P. A. M., Watts, N. L., Wilkie, J. T. 1993. Akaso Field, Nigeria: Use of integrated 3-D seismic, fault slicing, clay smearing, and RFT pressure data on fault trapping and dynamic leakage. AAPG Bulletin, 77(8), 1389-1404.

Johannesen, J., Hay, J., Milne,J.K., Jebsen,C.,Gunnesdal,S.C., Vayssaire,A. 2002. 3D oil migration modelling of the Jurassic petroleum system of the Statfjord area, Norwegian North Sea. Petroleum Geoscience, 8(1), 37-50

Kauerauf, A., Hantschel, T., Tscherney, R., Better prediction of fluid-flow modelling – multi-component modelling of petroleum migration and acculmulation. In: AAPG Hedberg Conference: Basin modelling perspectives: innovative developments and novel applications. Abstract only.

Kim, J., Berg, R. R., Watkins, J. S., Tieh, T. T. 2003. Trapping capacity of faults in the Eocene Yegua Formation, East Sour Lake field, southeast Texas. AAPG Bulletin, 87(3), 415-425.

Krokstad, W., Sylta, Ø. 1996. Risk assessment using volumetrics from secondary migration modelling: assessing uncertainties in source rock yields and trapped hydrocarbons, in: A.G. Dore and R. Sinding-Larsen (Eds), Quantifiaction and Prediction of Petroleum Resources. Norwegian Petroleum Society (NPF), Special Publication 6, Trondheim, Norway, pp. 219-235.

Lindsay, N. G., Murphy, F. C., Walsh, J. J., Watterson, J. 1993. Outcrop studies of shale smears on fault surfaces, in: Flint, S., Bryant, I. D. (Eds), The Geological Modelling of Hydrocarbon Reservoirs and Outcrop Analogues. Special Publication of the International Association of Sedimentologists, 15, pp. 113-123.

Perkins, H. 1961. Fault closure-type fields, southeast Louisiana. Transactions of the Gulf Coast Association Geological Society. 11, 177-196.

Sperrevik, S., Gillespie, P. A., Fisher, Q. J., Halvorsen, T., Knipe, R. J. 2002. Empirical estimation of fault rock properties. in: Koestler, A.G., Hunsdale, R. (Eds), Hydrocarbon Seal Quantification. Norwegian Petroleum Society (NPF), Special Publication 11, Trondheim, Norway, 109-126.

Stewart, I. J., Rattey, R. P., Vann, I. R. 1992. Structural style and the habitat of hydrocarbons in the North Sea, in: Larsen, R. M., Brekke, H., Larsen, B. T., Talleraas, E. (Eds), Structural and Tectonic Modelling and its Implications to Petroleum Geology. Norwegian Petroleum Society (NPF), Special Publication 1, Trondheim, Norway, pp. 197-220.

Sylta, Ø. 1991. Modelling of secondary migration and entrapment of a multicomponent hydrocarbon mixture using equation of state and ray-tracing modelling techniques, in: W.A. England and A.J. Fleet (Eds), Petroleum Migration. Geological Society London Special Publication 59, pp. 111-122.

Sylta Ø. 2004. A probabilistic approach to improved geological knowledge and reduced exploration risks using hydrocarbon migration modeling. Petroleum Geoscience, 10(3), 187-198.

Tabor, J. R., Busch J. P., Dula, W. F., Naruk, S. J. 2003. Fault seal controls on gas column heights, offshore Netherlands, southern North Sea. Abstract In ‘Faults and Top Seals’ meeting of European Association of Geoscientists and Engineers, Montpellier.

Watts, N. L. 1987. Theoretical aspects of cap-rock and fault seals for single- and two-phase hydrocarbon columns. Marine and Petroleum Geology, 4(4), 274-307.

Weber, K. J., Mandl, G., Pilaar, W. F., Lehner, F., Precious, R. G. 1978. The role of faults in hydrocarbon migration and trapping in Nigerian growth fault structures. In:

10th Annual Offshore Technology Conference 4. Society of Petroleum Engineers, 2643-2653.

Yielding, G., Freeman, B., Needham, D. T. 1997. Quantitative fault seal prediction. AAPG Bulletin, 81(6), 897-917.

Figure Captions

Fig. 1. (A) Map of the Northern North Sea showing the location of the Oseberg Syd Field (after Stewart et al. 1992). (B) Map of the Oseberg Syd area showing well locations and known hydrocarbon accumulations. The fault pattern shown is a simplified version of the mid-Tarbert fault pattern used in the migration models. The faults shown in black are those used in the single-fault seal calibration (Fig. 3). The Oseberg Fault is labelled OF. The dashed line is the trace of the Cretaceous unconformity at the mid-Tarbert level and the trace of the cross-section in Fig. 5 is shown

Fig. 2. Structure contour map of the top Tarbert reservoir horizon; depths in kilometres. Black lines outline fault polygons used in the definition of the migration model. Also shown are oil accumulations (dark green) which result when the migration model is run with no capillary properties assigned to the faults i.e. fault seal capacity is defined only from the geometry of the top reservoir horizon. Open circles are the locations of the 7 calibration points used to compare model results with known hydrocarbon distributions.

Fig. 3. Plot of SGR versus buoyancy pressure for oil (open circles) and gas (filled circles) showing the results of the single-fault seal analysis exercise conducted for the Oseberg Syd area. The faults analysed are indicated in Fig. 1.

Fig. 4. (A) The three fault seal types considered in migration modelling. (B) and (C) illustrate the method of calculation of cross- and along-fault membrane seal capacity (see text).

Fig. 5. (A) Cross-section through the geological model shaded according to Vshale. The 5 horizons constraining the interpolation of Vshale between wells (shown black) are Top Tarbert Fm. (TT), Top Ness Fm. (TN) Top Oseberg Fm. (TO), Base Brent (BB) and Top Statfjord Fm. Note that Vshale is not defined within the fault polygons which are mapped at a mid-Tarbert reflector. (B) Sample Vshale curves from wells along the cross-section in (A). The shading is the same as in (A).

Fig. 6. Illustration of the 3 parameters which were varied to define different SGR versus fault rock threshold pressure realizations.

Fig. 7. Plots of SGR-onset versus slope of SGR versus fault rock threshold pressure relationship colour coded for misfit, for the seven individual calibration points (1 to 7) and the sum of all calibration points (All). The key in (1) is the same for (2) to (7). The points labelled A, B and C define the seal capacity parameters used in the model realizations shown in Fig. 8 (A to C). The areas outlined in black on the plot for Trap 3 define the parameter range for the 200 best fit realisations for the remaining six traps (see text).

Fig. 8. Maps of oil distribution for part of the model for three different fault seal capacity envelopes. The SGR-onset and slope which define the seal capacity envelope for each of the three realizations is shown in Fig. 7. The open circle is the location of calibration point 5. The red curves show the main migration arteries in each realisation.

Fig. 9. Plots of the 3 parameters defining a SGR – fault rock threshold pressure relationship, or fault seal envelope, versus the total misfit.

Fig. 10. Plots of SGR versus fault rock threshold pressure showing (A) the straight line relationships input to each of 3,130 realisations and (B) the concave upwards relationships input to each of 835 realisations. In both cases only the inclined part of the fault seal envelope is shown and the plateau at the maximum threshold pressure is not shown. Open circles in (A) are results from the standard method of defining fault seal capacity for oil, see Fig. 3. Curves are coloured for misfit according to the key in A.

Fig. 11. Histograms of predicted trapped column height for each calibration point treating that trap as a prospect (see text). The histograms are for the 200 lowest misfit realisations calculated for all traps excluding the prospect trap. The vertical arrows in each histogram are the actual column heights in each trap. The black bins in each histogram are the

795 modal values of the largest data cluster in each histogram; these values are plotted in Fig.
796 12(A).
797
798 Fig. 12. (A) Plot of actual column height versus predicted column height for the 7 traps.
799 The predicted column heights are the modal values of the largest cluster in each of the
800 histograms in Fig. 11 (shown black in histogram) and the vertical bars are the range of the
801 largest each cluster. (B) Cross-plot of the heights of the oil columns in Trap 4 and Trap 2
802 for all 3 130 realisations. The large filled circle is a realisation for which both traps are
803 filled to their known heights.
804

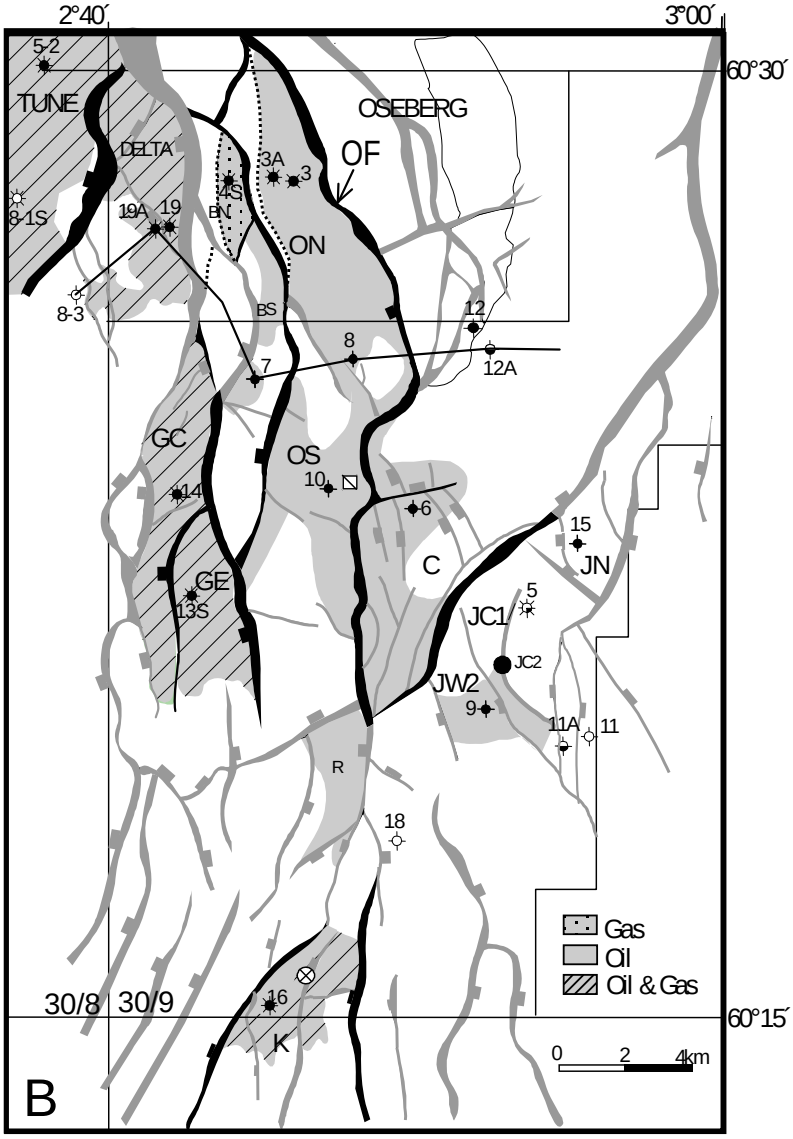
2°40´
3°00´
60°30´
60°15´
5-2
TUNE
DELTA
OSEBERG
OF
3A
3
4S
BN
ON
8-1S
19A
19
8-3
BS
12
12A
8
7
GC
OS
10
14
6
15
JN
C
GE
13S
5
JC1
JC2
JW2
9
11A
11
R
18
16
K
30/8
30/9
Gas
Oil
Oil & Gas
0
2
4km
B

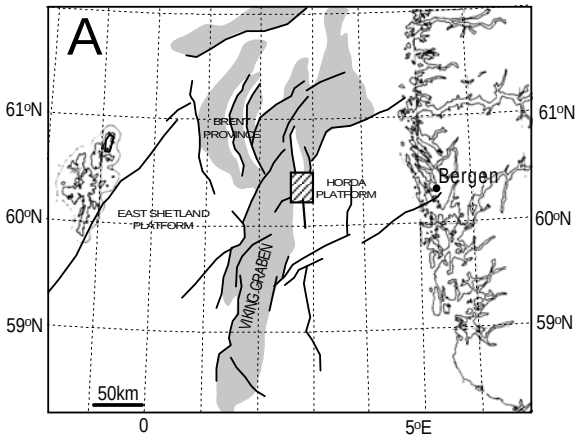
A
61ºN
60ºN
59ºN
5ºE
BRENT PROVINCE
HORDA PLATFORM
Bergen
EAST SHETLAND PLATFORM
VIKING GRABEN
50km
0

Figure 1

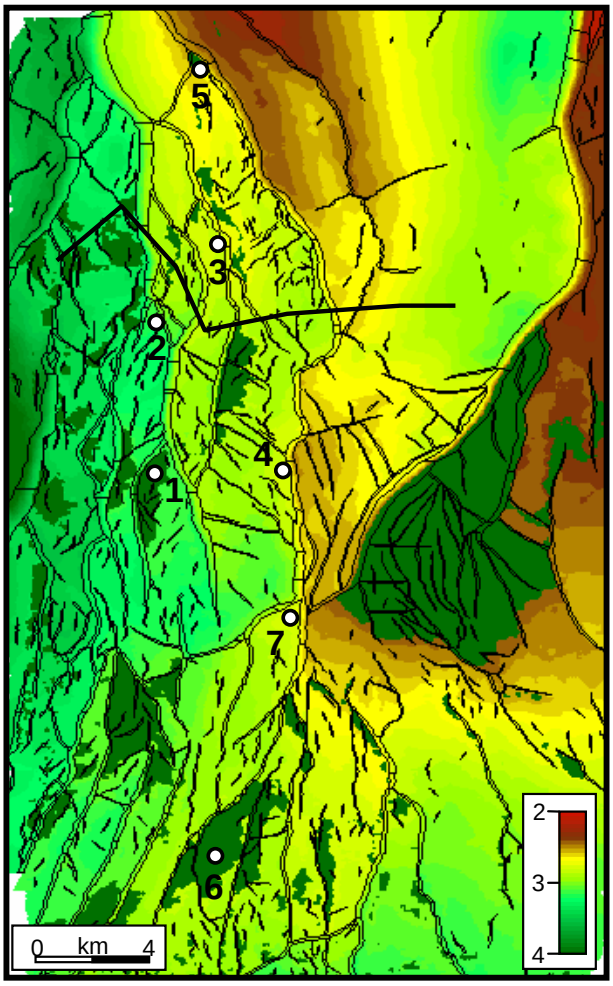

Figure 2

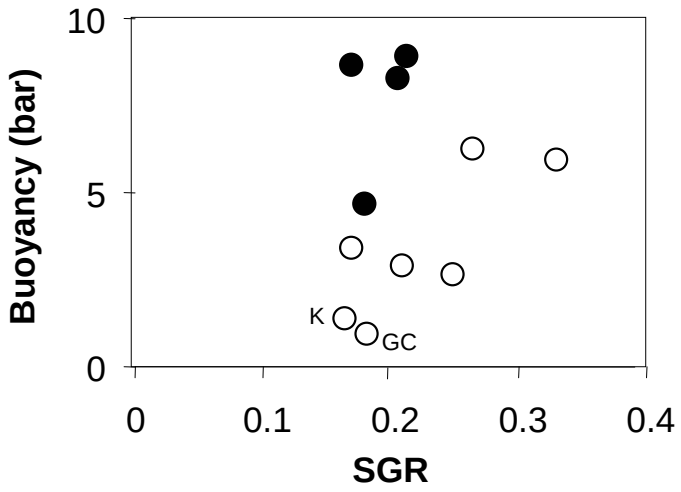

Figure 3

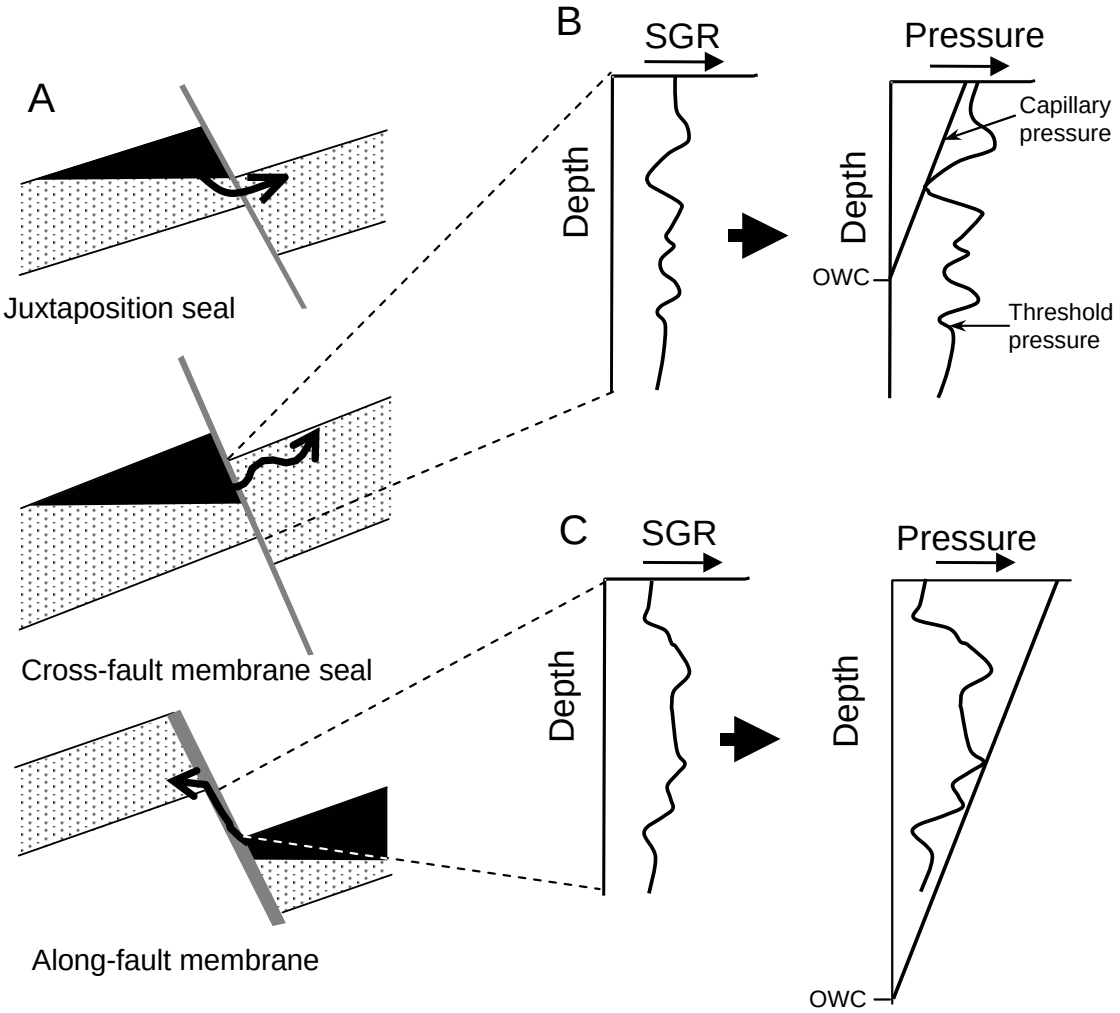
A
Juxtaposition seal
Cross-fault membrane seal
Along-fault membrane
B
SGR
Depth
Pressure
Depth
Capillary
pressure
OWC
Threshold
pressure
C
SGR
Depth
Pressure
Depth
OWC

Figure 4

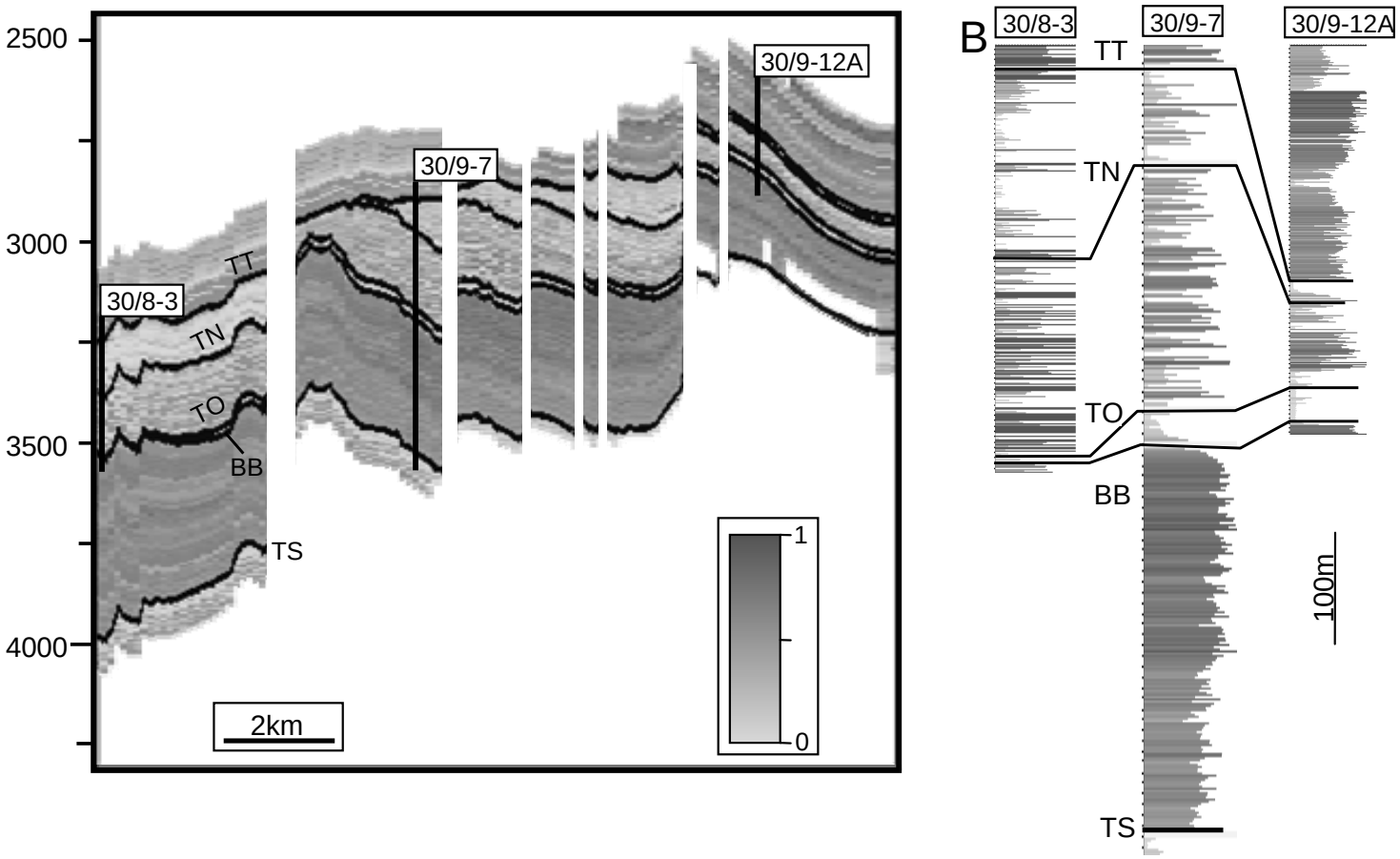
2500
3000
3500
4000
30/8-3
30/9-7
30/9-12A
TT
TN
TO
BB
TS
2km
1
0
B
30/8-3
30/9-7
30/9-12A
TT
TN
TO
BB
TS
100m

Figure 5

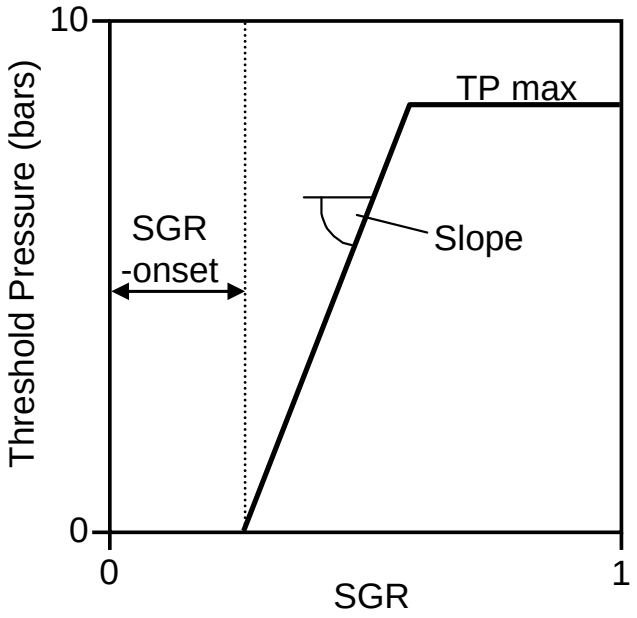

Figure 6

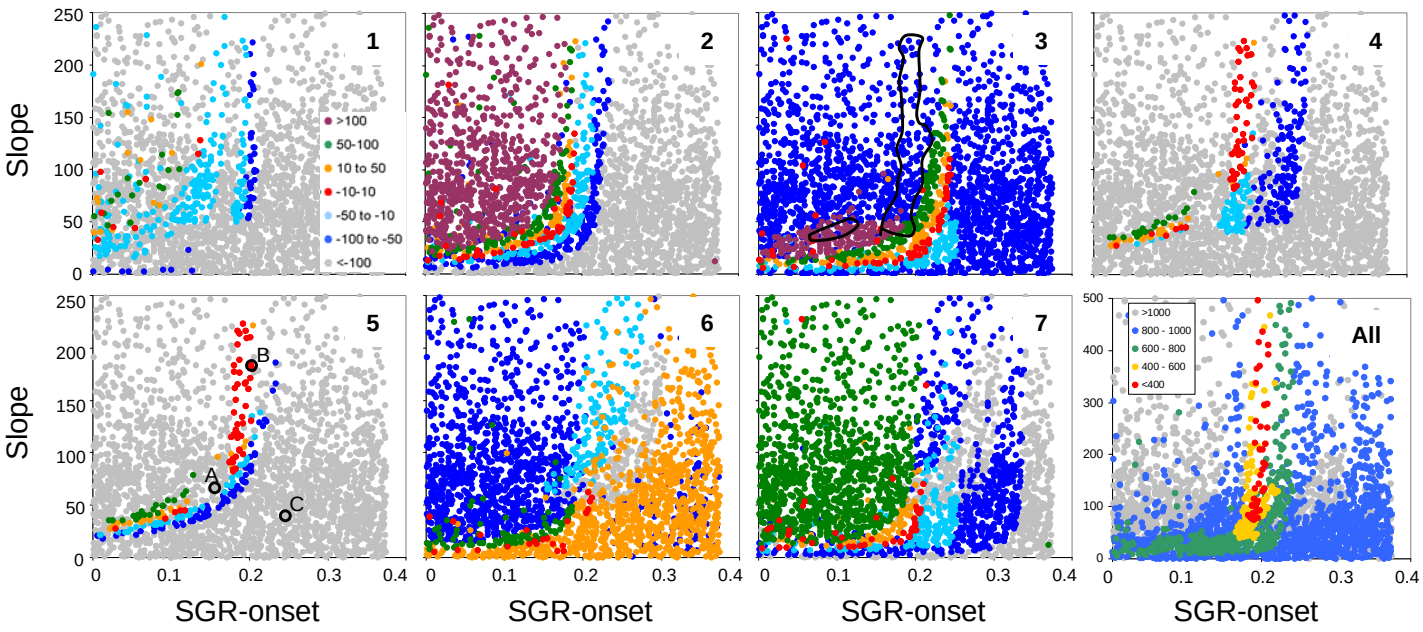
Slope
SGR-onset
1
2
3
4
5
6
7
All
>100
50-100
10 to 50
-10-10
-50 to -10
-100 to -50
<-100
>1000
800 - 1000
600 - 800
400 - 600
<400
A
B
C

Figure 7

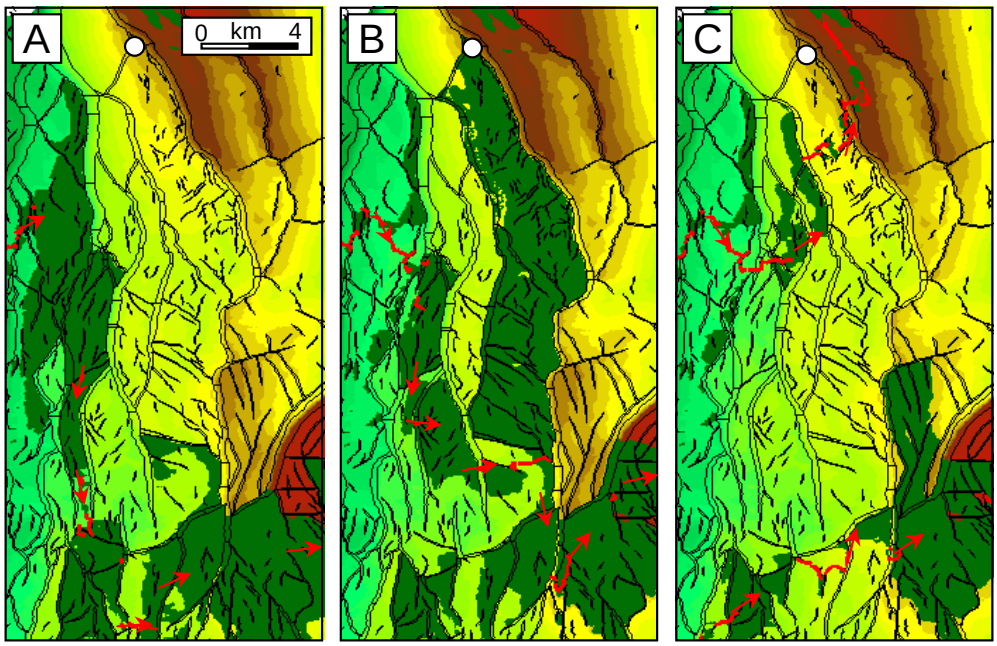

High fault seal capacity
(low SGR-onset)

Low fault seal capacity
(high SGR -onset)

Figure 8

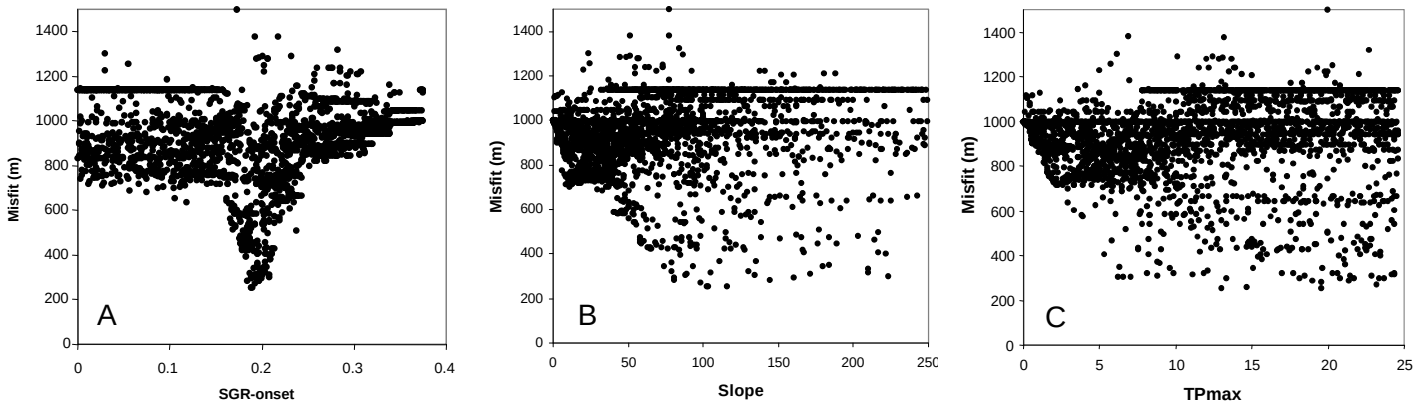
Misfit (m)
1400
1200
1000
800
600
400
200
0
0
0.1
0.2
0.3
0.4
SGR-onset
A
Misfit (m)
1400
1200
1000
800
600
400
200
0
0
50
100
150
200
250
Slope
B
Misfit (m)
1400
1200
1000
800
600
400
200
0
0
5
10
15
20
25
TPmax
C

Figure 9

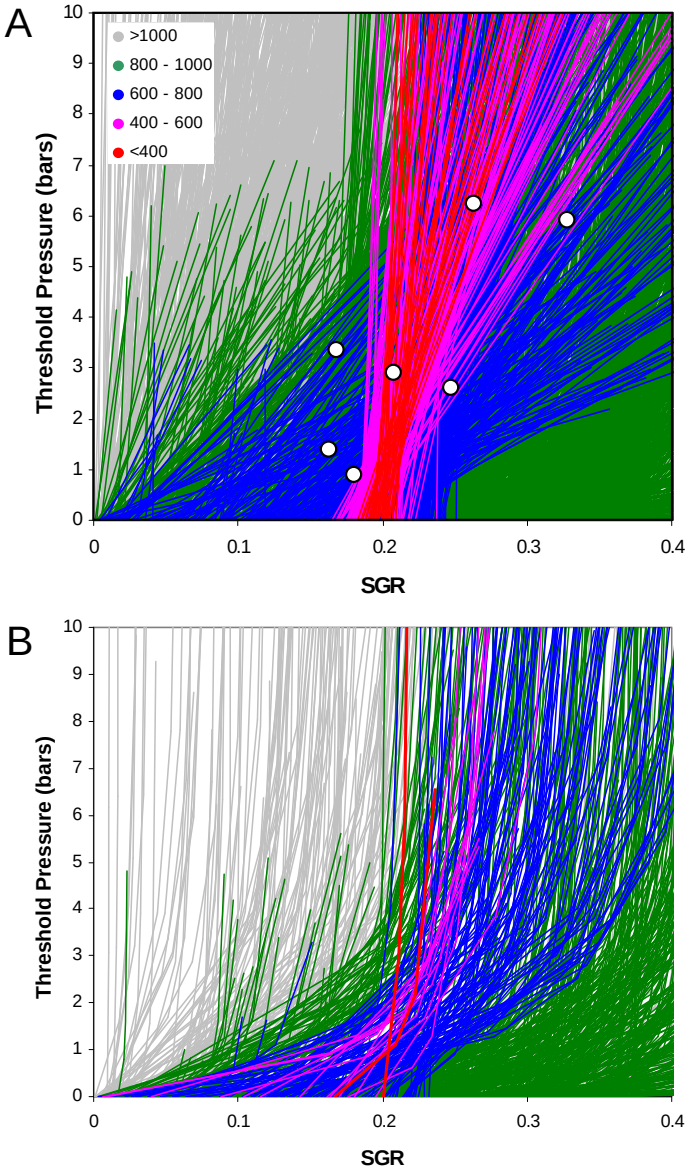
A
>1000
800 - 1000
600 - 800
400 - 600
<400
Threshold Pressure (bars)
SGR
B
Threshold Pressure (bars)
SGR

Figure 10

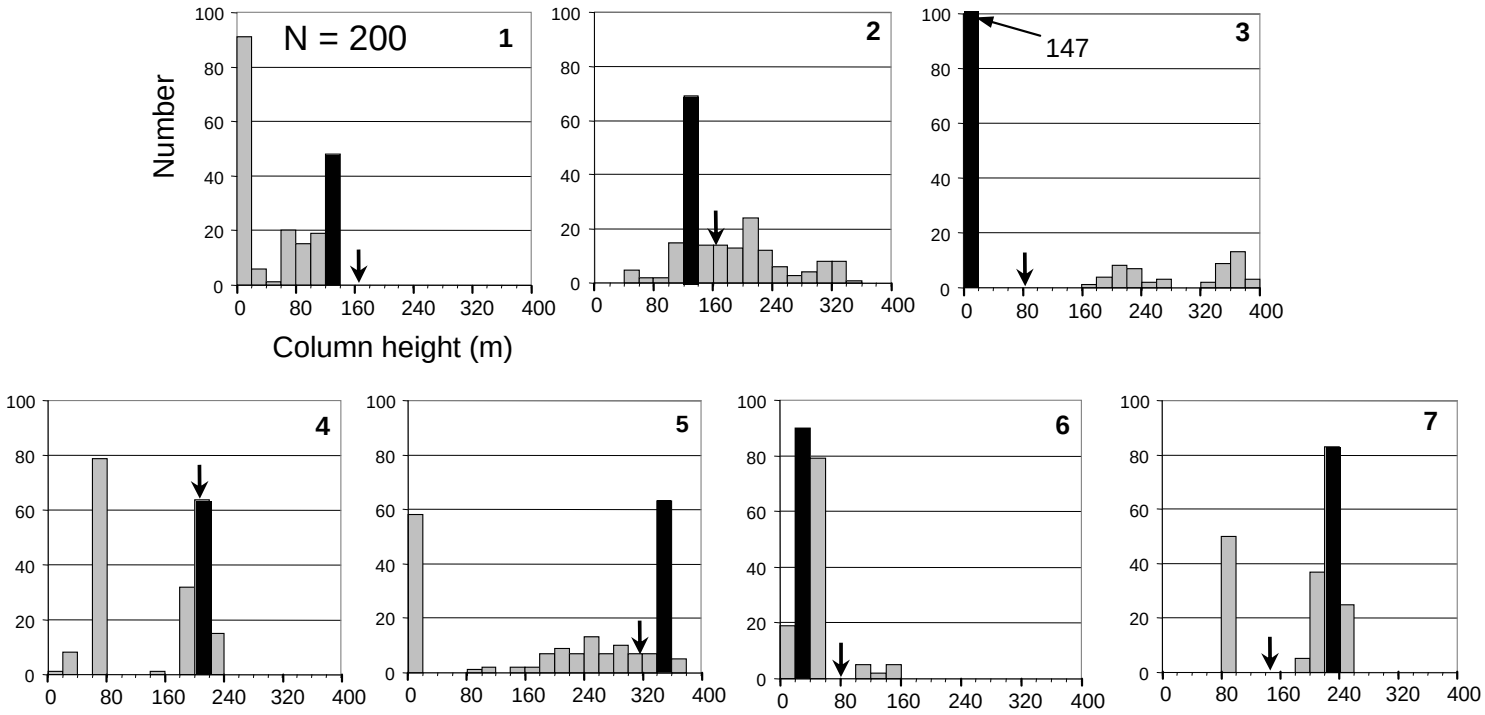

Figure 11

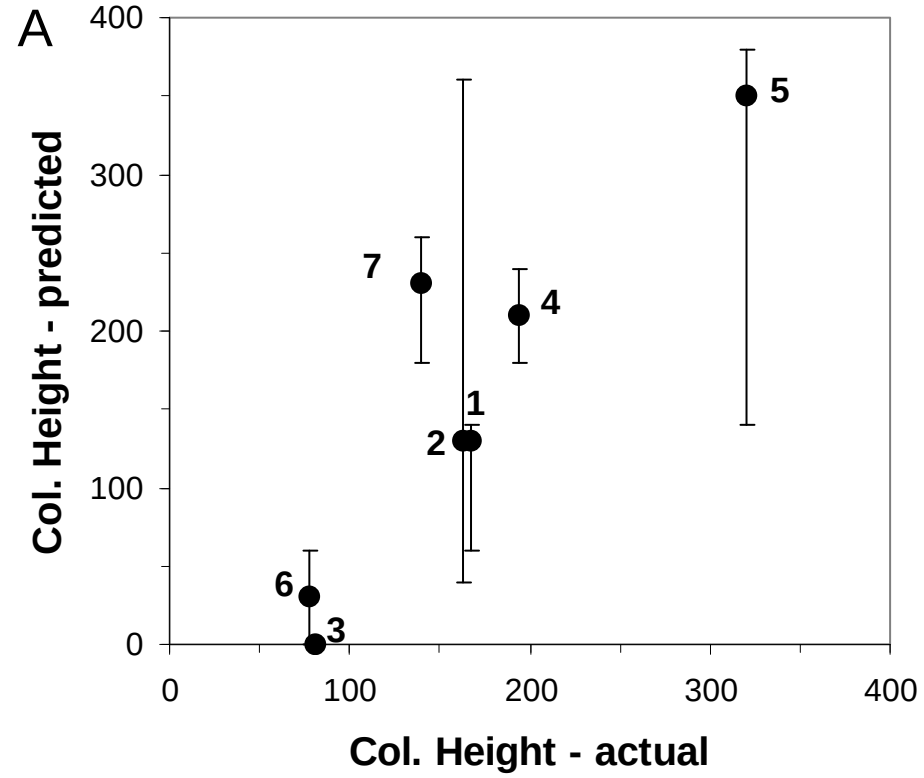
A
Col. Height - predicted
Col. Height - actual
0
100
200
300
400
1
2
3
4
5
6
7

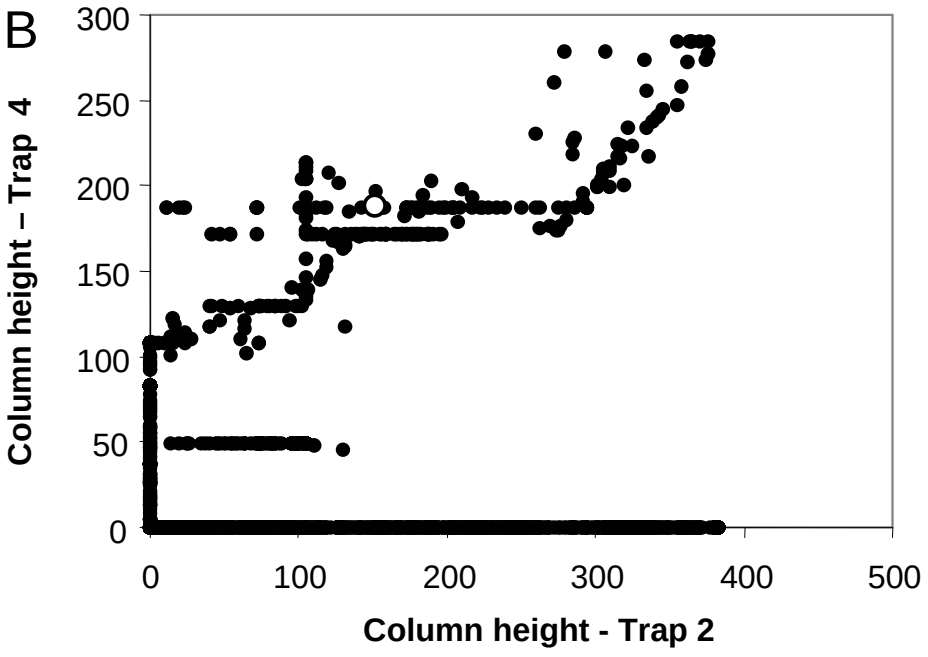
B
Column height – Trap 4
Column height - Trap 2
0
50
100
150
200
250
300
400
500

Figure 12